Received 17 January 2022
Revised 29 February 2022
Accepted 14 April 2022

Research on rail wear of small radius curve in EMU depot

Hao Li
The Ministry of Construction, China Railway Guangzhou Bureau Group Co., Ltd, Guangzhou, China
Jialin Sun
Infrastructure Testing Institute, China Academy of Railway Sciences Corporation Limited, Beijing, China, and
Guotang Zhao
Ministry of science, Technology and Information Technology, China State Railway Group Co., Ltd, Beijing, China

Abstract

Purpose – With the help of multi-body dynamics software UM, the paper uses Kik–Piotrowski model to simulate wheel-rail contact and Archard wear model for rail wear.
Design/methodology/approach – The CRH5 vehicle-track coupling dynamics model is constructed for the wear study of rails of small radius curves, namely 200 and 350 m in Guangzhou East EMU Depot and those 250 and 300 m radius in Taiyuan South EMU Depot.
Findings – Results show that the rail wear at the straight-circle point, the curve center point and the circle-straight point follows the order of center point > the circle-straight point > the straight-circle point. The wear on rail of small radius curves intensifies with the rise of running speed, and the wearing trend tends to fasten as the curve radius declines. The maximum rail wear of the inner rail can reach 2.29 mm, while that of the outer rail, 10.11 mm.
Originality/value – With the increase of the train passing number, the wear range tends to expand. The rail wear decreases with the increase of the curve radius. The dynamic response of vehicle increases with the increase of rail wear, among which the derailment coefficient is affected the most. When the number of passing vehicles reaches 1 million, the derailment coefficient exceeds the limit value, which poses a risk of derailment.

Keywords EMU depot, Small radius curve, Rail wear, Vehicle-track coupling dynamics, Dynamic response
Paper type Research paper

1. Introduction

As trains run on railway tracks, the rolling and slipping occurred between the wheel and rail tend to incur wear to both, with small radius curves being a very distinctive example of such hazard. The complex issue of wheel-rail wear involves many factors, such as the structural forms of the train and track, materials of wheel-rail system, wheel-rail interaction mode, temperature, humidity and stimulation of various effects (Lewis & Olofsson, 2009). From the perspective of track maintenance, rail wear poses an important form of rail defects (Zou, Yang, Lu, & Xing, 2010), directly related to operation safety and maintenance costs of the wheel-rail system. Domestic and foreign researchers have made extensive studies for a long

Fund project: Project funded by National Natural Science Foundation of China (51778050) and Task of Science and Technology R&D Program of China Railway Corporation (P2018G003).

Railway Sciences
Vol. 1 No. 1, 2022
pp. 16-39
Emerald Publishing Limited
e-ISSN: 2755-0915
p-ISSN: 2755-0907
DOI 10.1108/RS-04-2022-0014

time. The paper gets 2,551 results on Web of Science, a foreign search engine, by entering the search subject "rail wear", as shown in Figure 1, while 961 results from "CNKI", a domestic search engine at eight resource libraries (including academic journals (716), academic dissertations (150), conferences (39), yearbooks (4), patents (25), standards (1), achievements (7) and special journals (19), as shown in Figure 2.

It can be seen from the search results that since the 21st century, significant progress has been made in domestic and foreign researches on rail wear, and the number of publications increases rapidly. The comprehensive analysis on existing literature leads to a rough categorization as follows: site investigation and test of rail wear (Deters & Proksch, 2004; Lewis *et al.*, 2019; Su *et al.*, 2019; Hu *et al.*, 2020): for example, Ludger Deters and Matthias Proksch tested the friction and wear between wheel and rail materials; theoretical analysis on rail wear (Sladkowski & Sitarz, 2004; Zhao & Zeng, 1995; Ramalho, 2015; Asih, Ding, & Kapoor, 2012; Zhu, Zeng, Zhang, & Yi, 2019): for example, Aleksander Sladkowski and Marek

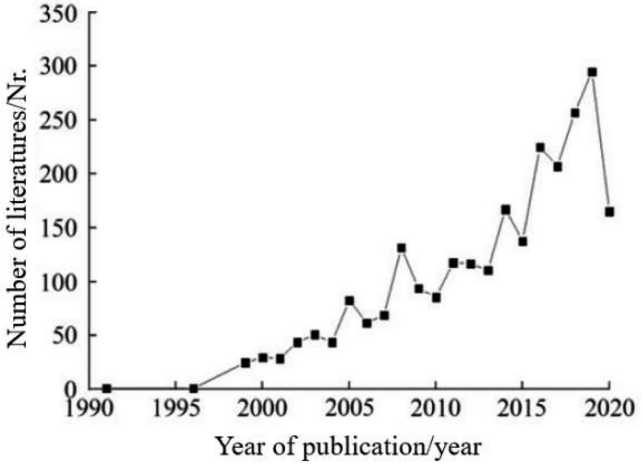

Figure 1.
Number of foreign literature on "rail wear"

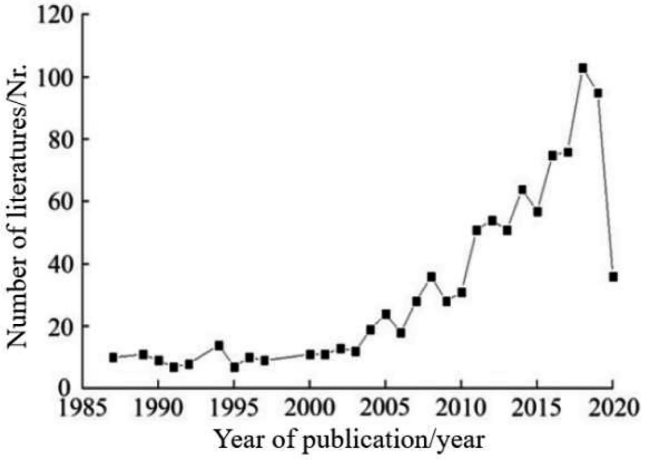

Figure 2.
Number of domestic literature on "rail wear"

Sitarz studied the wheel-rail contact relation and the two-point contact between the two with finite element software Ansys, and based on these researches, they think that severe wear would occur on the wheel flange in case of two-point contact; prediction of rail wear and life expectance left (Dang & Maitournam, 2002; Meehan, Daniel, & Campey, 2005; Wang, Wang, Wang, & Liu, 2011; Ding, Lewis, Beagles, & Wang, 2018; Pavlík, Gerlici, & Lack, 2019; Khan, Persson, Lundberg, & Stenstrom, 2017): for example, Dang Van K and Maitournam M H predicted the trends of rail fatigue and wear with the help of finite element analysis, converted the pressure distribution on rail top into spherical pressure distribution on equivalent plastic volume using 2D finite element and Fourier transform, and finally predicted the fatigue and wear of rail surface at different loading points via the calculation of fatigue distribution.

It can be seen from above that researchers mainly took operational lines as the study objects for rail wear, while limited focus was given to the rail wear occurred to EMU running track and EMU depot which do not take passenger transport tasks but register a large amount of small radius curves, generally 200–350 m (Feng, 2018). In this context, the paper takes on the rail wear of small radius curve in EMU depot as the research subject.

2. Analysis model of rail wear of small radius curve

The analysis model of rail wear of small radius curve constructed includes four parts, namely vehicle-track coupling dynamics model, wheel-rail contact model, material wear model and profile renewal processing.

2.1 Vehicle-track coupling dynamics model

The vehicle-track coupling dynamics model of CRH_5 EMU is constructed based on multi-body dynamics software UM, as shown in Figure 3. With one carbody, two bolsters, two frames, four wheelsets and eight axle boxes, the vehicle records 62 in total degrees of freedom, including 6 degrees of freedom for the body, bolster, frame and wheelset, while only that of head nodding is considered for the axle box. The primary and the secondary suspensions are simulated with linear or nonlinear spring-damping force elements in accordance with actual vehicle structure. The primary suspension mainly includes primary spring, primary damping and tumbler node, while the secondary suspension, the air spring, transverse damper, anti-hunting damper, traction rod, transverse stop, etc.

Line 1 is *R*200 m and *R*350 m inverse curves on No. 19 passenger rail at EMU depot in Guangzhou East Station, with the cross-section and profile of the line shown in Figure 4. Line 2 is *R*250 m and *R*300 m inverse curves on No. 16 passenger rail at EMU depot in Taiyuan South Station, with the cross-section and profile of the line shown in Figure 5. For a realistic simulation of the flexible characteristic of the track, the paper chooses finite element method to simulate 3D Timoshenko beam as the rail.

2.2 Wheel-rail contact model

The wheel-rail contact model constitutes an important part for the interaction of wheel and rail. Traditional FASTSim model is a single-point contact model constructed based on Hertz ellipse theory. Despite the wide application of this model, the wheel-rail profile tends to form a conformal contact as the wheel or rail wear reaches a certain level where the single-point contact turns into a multipoint one. This is particularly true when it comes to small radius curves, therefore any persisting efforts to apply this model seem irrational. The CONTACT

Figure 3.
Vehicle-track coupling dynamics model of CRH_5 EMU

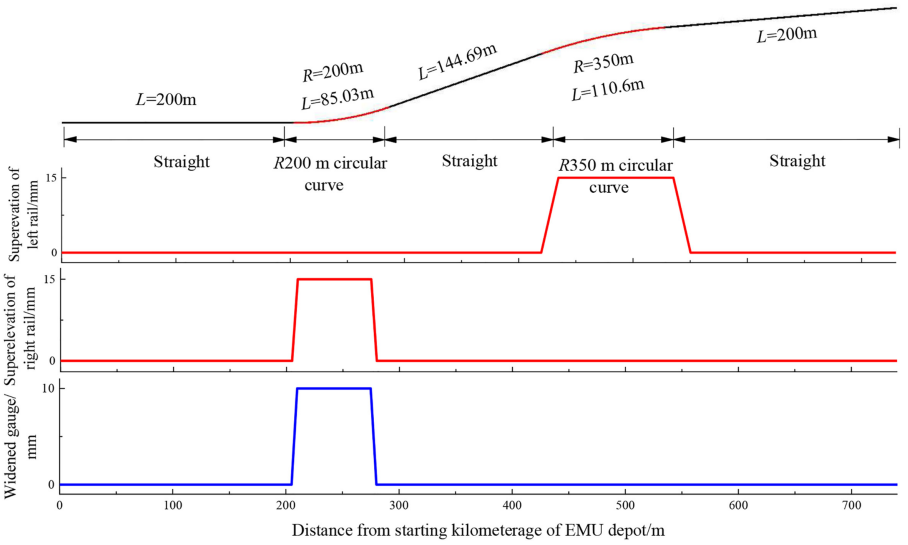

Figure 4.
Cross-section and profile of line with *R*200 m and *R*350 m circular curves

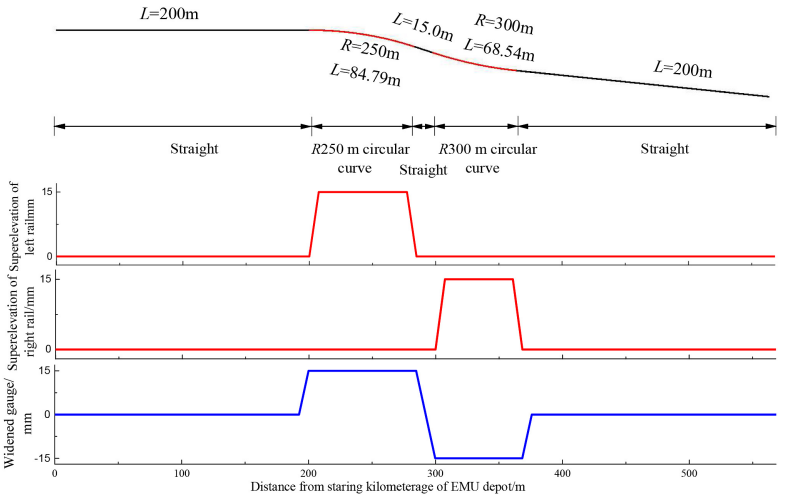

Figure 5.
Cross-section and profile of line with *R*250 m and *R*300 m circular curves

precision theory developed by Kalker is the best option (Kalker, 1990) when it comes to wheel-rail contact, but the calculation efficiency turns out to be unsatisfying. In this light, the paper chooses Kik–Piotrowski model (Piotrowski & Chollet, 2005), which promises both the calculation precision of CONTACT and great calculation efficiency, while avoiding the calculation error caused by abnormal curvature fluctuation.

2.3 Archard wear model

Domestic and foreign scholars have made extensive studies on material wear and come up with different calculation models, among which the Archard model, Specht model and

Plasticity model (Lin, 2014) are the top choices. The paper chooses the Archard wear model which is constructed on the premise that volume wear and the work of creep force register a linear relation.

The frictional contact area A_r is made up of cross-sectional area of micro-convexs with a radius of r, as shown below.

$$A_r = n\pi r^2 \tag{1}$$

where n is the number of micro-convexs.

In case where no slipping occurs, the total number of collisions between micro-convexs Np is as follows:

$$N_p = \frac{F}{\pi r^2 \sigma_s} \tag{2}$$

where F is the load acting on the contact area and σ_s is the plastic flow stress of the material.

In relative slipping, it is assumed that a piece of hemispherical wear debris is produced in every $2r$ displacement, therefore wear V_w produced by the slipping of s can be evaluated by the following equation:

$$V_w = N_p \frac{s}{2r} \frac{2}{3} k\pi r^3 = \frac{k}{3} \frac{F}{\sigma_s} s \tag{3}$$

where k is the wear coefficient.

It can be seen from the theory of elastic mechanics that for metal materials, hardness H maintains a certain correlation with σ_s, namely

$$H = 3\sigma_s \tag{4}$$

Therefore, Equation (3) can be written as follows:

$$V_w = k\frac{sF}{H} \tag{5}$$

The wear coefficient k has many impact factors, among which the friction temperature, imposed load, material and rolling speed have great impact, most of which are determined via tests. The research results of Reference (Olofsson & Telliskivi, 2003; Jendel & Berg, 2002) indicate that the most severe wear occurs in areas where $p > 0.8H$. It needs to be noted that p is the normal compressive stress on the contact surface, while H, the hardness of the softer material of contact. In this case, k is 0.03–0. 04.

According to the Coulomb law of friction, the equation of slipping friction force is as follows:

$$F_f = \mu F_N \tag{6}$$

where F is slipping friction; μ is dynamic friction coefficient and F_N is the normal force.

Therefore, Equation (5) can be expressed as follows:

$$V_w = k\frac{sF_N}{H} = k\frac{sF_f}{\mu H} \tag{7}$$

It is also known that frictional work W can be expressed as follows:

$$W = sF_f \tag{8}$$

Since k, μ and H are all material-related parameters, it is assumed that

$$K = \frac{k}{\mu H} \tag{9}$$

The following equation can be obtained by substituting Equations (8) and (9) into Equation (7):

$$V_w = KW \tag{10}$$

According to Archard wear model (Lin, 2014; Olofsson & Telliskivi, 2003; Jendel & Tomas, 2002), wear does not occur at the adhesion area of the contact surface due to the lack of relative slipping. Therefore, $V_{w,s}$ and F in Equation (5) can be expressed as follows:

$$V_w = \int_{\Delta t} \dot{h} A dt \tag{11}$$

$$s = \int_{\Delta t} v_{\text{slip}} dt \tag{12}$$

$$F = pA \tag{13}$$

where $\dot{h}$ is the wear speed of the discrete point along the depth direction; A is the contact area and v_{slip} is the relative slip speed at wheel-rail contact surface.

The wear speed of discrete point can be obtained in accordance with Equations (5) and (10)–(13), namely

$$\dot{h} = k \frac{v_{\text{slip}} p}{H} \tag{14}$$

The wear depth Δh of the discrete point can be obtained as follows via time integration for Equation (14):

$$\Delta h = \int_{\Delta t} k \frac{v_{\text{slip}} p}{H} dt \tag{15}$$

Therefore, Equation (15) can be converted into the following in accordance with Equations (8) and (10):

$$\Delta h = \int_{\Delta t} K (v_{\text{slip}} F_f) dt \tag{16}$$

The friction power across the contact area can be obtained by the integration of the friction power of all units at the wheel-rail contact area, and the frictional work and wear volume can be further obtained by extended integration. The current wear on the rail profile is located via the combination of the wear volume and position of the contact point. Iterative calculation is used to realize the wear evolution on the rail profile. When the normal depth of rail wear or the number of passing vehicles reaches the set value during iterative calculation, current iteration is terminated. The profile obtained via smoothness processing is used as the initial profile for the next iteration to realize profile renewal. It is set that wear occurs 7.5 m before and after the straight-circle point, center point and circle-straight point (a range of 15 m) are collected for analysis, together with the profile at the above-mentioned characteristic points. According to the trial calculation, the paper chooses 10,000 round trips of vehicles/trains as the premise for iteration.

3. Rail wear characteristics of small radius curve in EMU depot

Given the different running speeds (15, 20, 25 and 30 km·h^{-1}) and the numbers of passing vehicles/trains (100,000, 200,000, 300,000, 400,000, 500,000, 600,000, 700,000, 800,000, 900,000 and 1 million vehicles), the paper conducts analysis on rail wear characteristics of *R*200 m, *R*250 m, *R*300 m and *R*350 m small radius curves in EMU depot.

3.1 R200 m small radius curve in Guangzhou East Station

Figure 6 shows the accumulative wears as different numbers of vehicles pass through the straight-circle point of *R*200 m small radius curve at 30 km·h^{-1}. It can be seen that wears accumulated to the inner rail wear of *R*200 m small radius curve are found mainly on the right side of the centerline of the cross-section, with the most severe wear mainly locating at 7.5 mm; while the outer rail wear concentrates on the left side of the centerline with the most severe hazard locating at 30.8 mm. It needs to be noted that in the case of the latter, the most severe wear has exceeded the 23 mm arc length of the *R*300 mm curve at the railhead and entered (*R*13 mm) connecting arc between rail top and rail side; the wear of the outer rail of the curve exceeds that of inner rail both in extent and range, covering the entire top width on the left of the centerline, and there are two wear waveforms on the connecting line between connecting points of two top arcs, but only slight wear is found at connecting points. Similar phenomenon also occurs in other working conditions; rail wear worsens as more vehicles/trains pass by.

The center point and the circle-straight point deliver similar wear characteristics. Figure 7 shows the maximum accumulative wear when different numbers of vehicles (100,000, 200,000, 300,000, 400,000, 500,000, 600,000, 700,000, 800,000, 900,000 and 1 million vehicles) pass through the straight-circle point, center point and circle-straight point of the *R*200 m small radius curve in EMU depot of Guangzhou East Station at different speeds (15, 20, 25 and 30 km ·h^{-1}); Table 1 shows the extend and the position of the maximum wear, as well as the wear range at the straight-circle point, center point and circle-straight point of the *R*200 m small radius curve when the number of vehicles passing through the curve reaches its limit.

The following conclusions can be drawn from Figure 7 and Table 1.

(1) When the same number of vehicles passes through *R*200 m small radius curve, the wear severity at the side rail of the curve decreases in the order of the center point, circle-straight point and straight-circle point.

(2) When one million vehicles/trains pass, the inner rail wear at the straight-circle point is 1.06 mm with the maximum wear speed of 15 km · h^{-1} and the outer rail wear is 1.49 mm with the maximum wear speed of 30 km · h^{-1}; inner and outer rail wears at the center point of the curve are 1.88 mm and 10.11 mm, respectively, with the maximum wear speed of 15 km · h^{-1}; the inner rail wear at the circle-straight point is 1.72 mm with the maximum wear speed of 15 km · h^{-1} and the maximum outer rail wear is 7.10 mm with the maximum wear speed of 25 km · h^{-1}.

(3) The most severe wear of the inner rail of the curve locates in 6.70–7.30 mm range with a few exceptions, while that of outer rail wear, in −34.70–−28.40 mm range.

(4) The inner rail wear at the straight-circle point locates in the range of −18.40–32.15 mm, while the outer rail wear locates in −35.05–16.35 mm range. The inner rail wear at the center point of the curve locates in −2.40–30.75 mm range and the outer rail wear locates in −35.05–17.40 mm range; the inner rail wear at the circle-straight point locates in −23.40–30.75 mm range and the outer rail wear locates in −35.00–16.40 mm range.

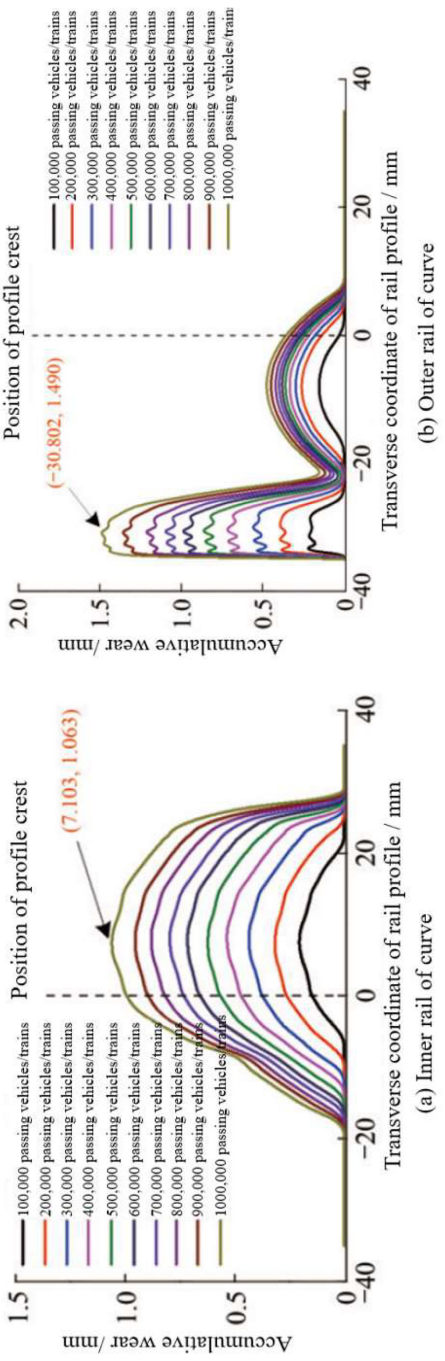

Figure 6.
Accumulative rail wears as different numbers of vehicles/trains pass through straight-circle point of *R*200 m small radius curve at 30 km•h^{-1}

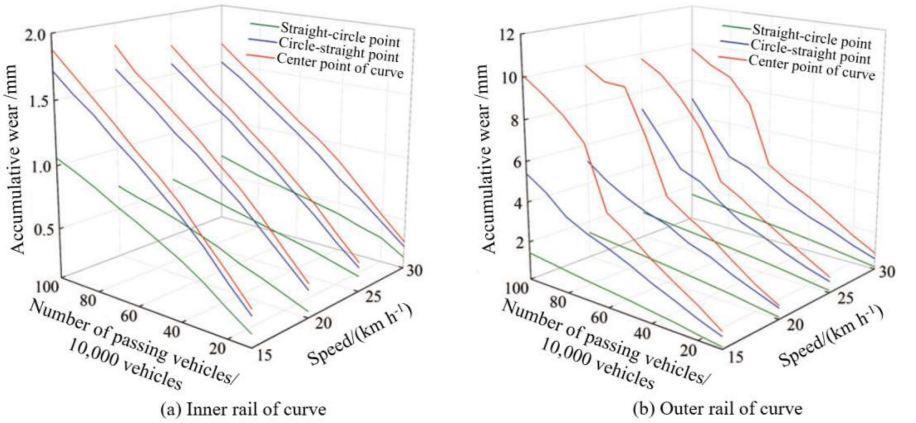

Figure 7.
Cumulative rail wear of *R*200 m small radius curve

		Inner rail of curve			Outer rail of curve		
Speed/ (km h^{-1})	Characteristic point of curve	Position of maximum wear/mm	Maximum wear/mm	Wear range/ mm	Position of maximum wear/mm	Maximum wear/mm	Wear r ange/mm
15	Straight-circle point	7.10	1.06	−18.40–30.00	−28.40	1.44	−35.05–16.35
	Center point of curve	7.00	1.88	−22.40–30.75	−34.65	10.11	−35.05–17.40
	Circle-straight point	6.75	1.72	−23.40–30.75	−34.50	5.40	−35.05–16.40
20	Straight-circle point	7.20	0.69	−14.40–29.20	−30.60	1.40	−35.05–11.40
	Center point of curve	7.30	1.83	−21.40–30.75	−34.70	9.97	−35.05–13.40
	Circle-straight point	6.70	1.64	−22.40–30.75	−34.50	5.15	−35.05–13.40
25	Straight-circle point	7.20	0.60	−12.40–29.20	−30.70	1.45	−35.05–10.40
	Center point of curve	10.15	1.74	−21.40–30.75	−34.65	9.73	−35.05–15.40
	Circle-straight point	6.75	1.59	−22.40–30.75	−34.60	7.10	−35.05–14.40
30	Straight-circle point	7.20	0.67	−13.40–32.15	−30.80	1.49	−35.05–10.40
	Center point of curve	6.80	1.67	−21.40–30.75	−34.70	9.70	−35.05–12.40
	Circle-straight point	6.80	1.51	−22.40–30.75	−34.60	0.97	−35.05–13.40

Table 1.
Maximum wear, position and range at characteristic points of *R*200 m small radius curve

3.2 R350 m small radius curve in Guangzhou East Station

Figure 8 shows the accumulative rail wear when different numbers of vehicles pass through the center point of R350 m small radius curve in EMU depot of Guangzhou East Station at 30 km h^{-1}.

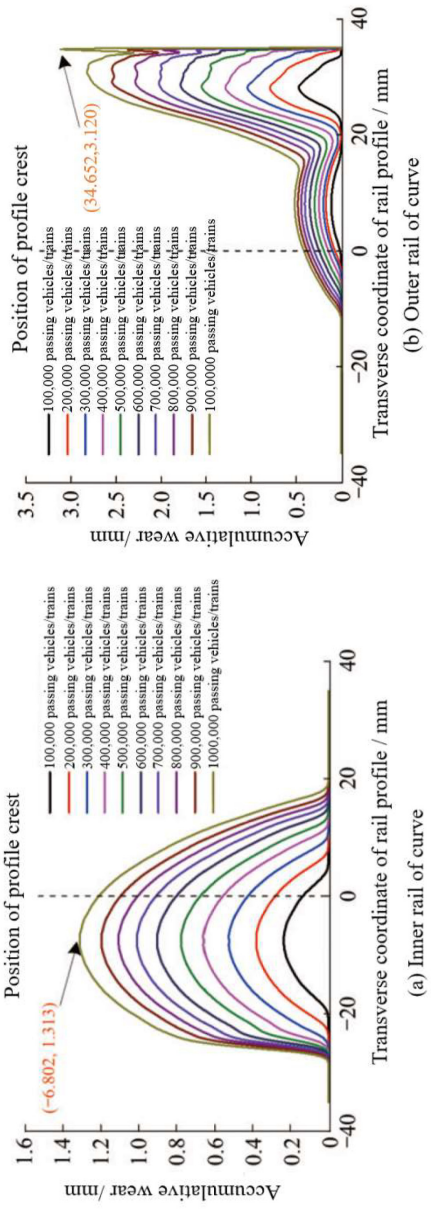

Figure 8.
Cumulative rail wears when different numbers of vehicles pass through center point of *R*350 m small radius curve at 30 km•h^{-1}

It can be seen from Figure 8 that outer rail wear of the curve mainly occurs on the right side of the centerline of the cross-section, with the maximum wear mainly in 28–35 mm range, which has exceeded the 23 mm arc length of *R*300 mm curve at the railhead and entered (*R*13 mm) the connecting arc between rail top and rail side; the inner rail wear mainly occurs on the left side of the centerline of the cross-section, with the maximum wear mainly occurring in 6.8–7.1 mm range; the outer rail wear exceeds inner rail wear, covering the entire top width on the right of the centerline, and there are two wear waveforms on the connecting line between connecting points of two top arcs, but the wear at connecting points is slight in comparison; rail wear increases as more vehicles/trains pass by.

The wear at the straight-circle point and that at circle-straight point can be quite similar. Figure 9 shows the maximum accumulative rail wear when different numbers of vehicles pass through the straight-circle point, center point and circle-straight point of *R*350 m small radius curve in EMU depot of Guangzhou East Station at different speeds; Table 2 shows the maximum rail wear, position and range at the straight-circle point, center point and circle-straight point of *R*350 m small radius curve when the number of vehicles/trains passing through the curve reaches the limit.

The following conclusions can be drawn from Figure 9 and Table 2.

(1) When the same number of vehicles passes through *R*350 m small radius curve, the wear severity at the side rail of the curve decreases in the order of the center point > the circle-straight point > the straight-circle point.

(2) When one million vehicles/trains pass, the inner and outer rail wear at the straight-circle point is 1.03 and 0.93 mm, respectively, with the maximum wear speed of 15 km · h^{-1}; inner rail wear at the center point of the curve is 1.31 mm with the maximum wear speed of 15 km · h^{-1} and the outer rail wear is 3.12 m with the maximum wear speed of 25 km · h^{-1}; the maximum inner rail wear at the circle-straight point is 1.32 mm with the maximum wear speed of 15 km · h^{-1} and the outer rail wear is 2.22 mm with the maximum wear speed of 30 km · h^{-1}.

(3) When an increasing number of vehicles passes through *R*350 m curve at different speeds, the maximum inner rail wear at straight-circle point locates in the range of −8.20–−7.05 mm with an average of −7.68 mm, and the maximum outer rail wear locates in the range of 8.00–28.10 mm with an average of 23.05 mm; the maximum inner rail wear at center point locates in the range of −8.30–−6.80 mm

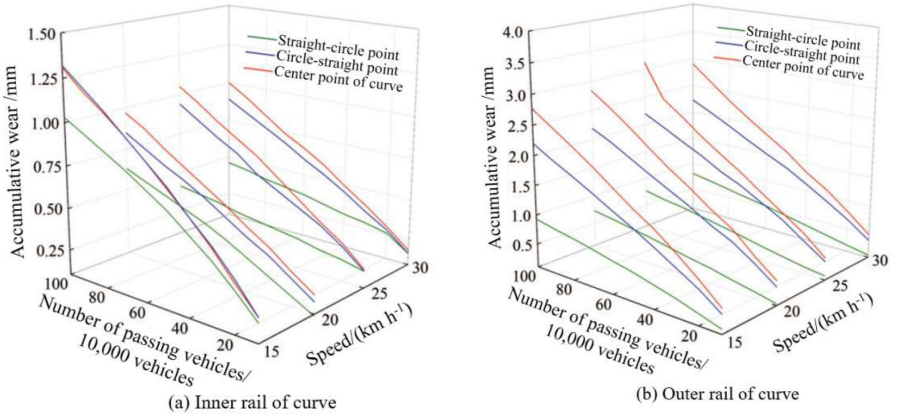

Figure 9.
Cumulative rail wear of *R*350 m small radius curve

Speed/ (km • h^{-1})	Characteristic point of curve	Inner rail of curve			Outer rail of curve		
		Position of maximum wear/mm	Maximum wear/mm	Wear r ange/mm	Position of maximum wear/mm	Maximum wear/mm	Wear r ange/mm
15	Straight-circle point	−8.20	1.03	−30.75–19.40	8.00	0.93	−18.40 –34.45
	Center point of curve	−6.80	1.31	−30.00–29.75	28.55	2.77	−13.35–35.05
	Circle-straight point	−6.80	1.32	−30.75–22.40	27.95	2.20	−14.40–35.05
20	Straight-circle point	−8.20	0.63	−30.00–14.40	28.00	0.73	−11.40–34.95
	Center point of curve	−8.30	0.97	−29.20–17.40	30.60	2.84	−7.40–35.05
	Circle-straight point	−8.15	0.85	−30.00–17.35	28.20	2.19	−7.40–35.05
25	Straight-circle point	−7.25	0.41	−29.20–10.40	28.10	0.77	−8.40–34.95
	Center point of curve	−6.80	1.05	−33.25–22.40	34.65	3.12	−14.40–35.10
	Circle-straight point	−8.30	0.94	−30.00–32.00	28.15	2.20	−10.40–35.05
30	Straight-circle point	−7.05	0.46	−29.20–11.40	28.10	0.79	−9.40–34.95
	Center point of curve	−6.80	1.00	−29.20–17.40	30.65	2.90	−10.40–35.05
	Circle-straight point	−8.20	0.89	−30.00–17.40	28.30	2.22	−10.40–35.05

Table 2. Maximum wear, position and range at characteristic points of *R*350 m small radius curve

with an average of −7.18 mm, and the maximum outer rail wear locates in 28.55–34.65 mm range with an average of 31.11 mm; the maximum inner rail wear at circle-straight point locates in −8.30–−6.80 mm range with an average of −7.86 mm, and the maximum outer rail wear locates in 27.95–28.30 mm range with an average of 28.15 mm. Generally speaking, the maximum inner rail wear locates at −7.57 mm on average, and the maximum outer rail wear locates at 27.44 mm on average.

(4) The inner rail wear at the straight-circle point locates in −30.75–19.40 mm range and the outer rail wear locates in −18.40–34.95 mm range; the inner rail wear at the center point of the curve locates in −33.25–29.75 mm range and the outer rail wear locates in −14.40–35.10 mm range; the inner rail wear at the circle-straight point locates in −30.75–32.00 mm range and the outer rail wear locates in −14.40–35.05 mm range.

3.3 R250 m small radius curve in Taiyuan South Station

Figure 10 shows the accumulative rail wear when different numbers of vehicles pass through the center point of *R*350 m small radius curve in EMU depot of Taiyuan South Station at 30 km h^{-1}. It can be seen from Figure 10 that the wear occurred to the outer rail of the curve far exceeds that to the inner rail, covering the entire top width on the right of the centerline, and there are two wear waveforms; rail wear increases as more vehicles/trains pass by.

The wear at the straight-circle point and that at circle-straight point bear similarity. Figure 11 shows the maximum accumulative rail wear when different numbers of vehicles

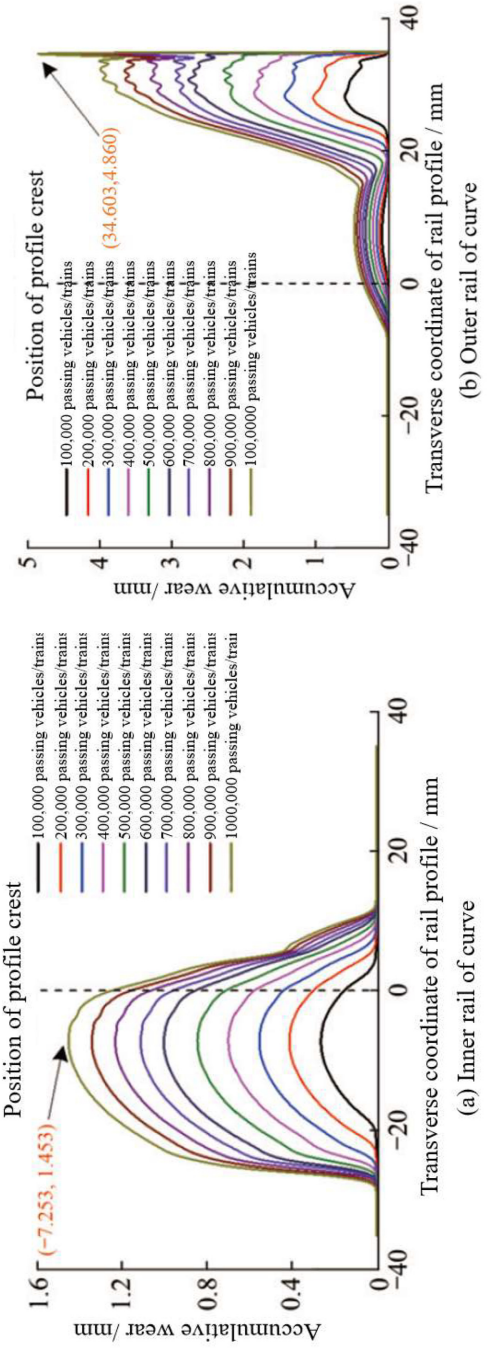

Figure 10.
Accumulative rail wears when different numbers of vehicles pass through center point of *R*250 m small radius curve at 30 km•h^{-1}

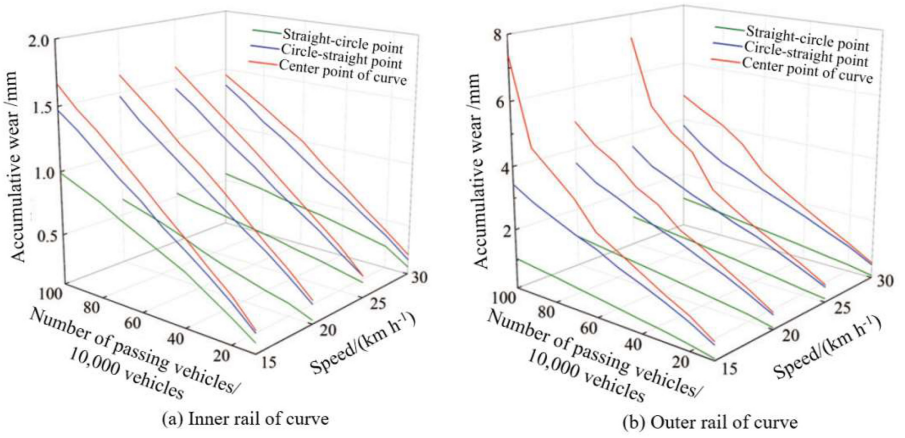

Figure 11.
Cumulative rail wear of *R*250 m small radius curve

pass through the straight-circle point, center point and circle-straight point of *R*250 m small radius curve in EMU depot of Taiyuan South Station at different speeds; Table 3 shows the maximum rail wear, position and range at the straight-circle point, center point and circle-straight point of *R*250 m small radius curve when the number of vehicles/trains passing through the curve reaches the limit.

		Inner rail of curve			Outer rail of curve		
Speed/ km • h^{-1})	Characteristic point of curve	Position of maximum wear/mm	Maximum wear/mm	Wear r ange/mm	Position of maximum wear/mm	Maximum wear/mm	Wear range/ mm
15	Straight-circle point	−6.95	0.99	−30.00–28.15	28.10	1.07	−17.40–35.00
	Center point of curve	−7.05	1.67	−30.75–16.40	34.60	7.40	−15.40–35.05
	Circle-straight point	−7.05	1.47	−30.00–16.40	34.55	3.44	−15.40–35.10
20	Straight-circle point	−8.20	0.63	−29.20–13.40	28.25	1.07	−12.40–35.00
	Center point of curve	−7.45	1.64	−30.00–15.40	34.50	4.90	−11.40–35.10
	Circle-straight point	−6.90	1.47	−30.00–15.40	34.55	3.55	−10.40–35.10
25	Straight-circle point	−6.90	0.53	−30.00–11.40	28.30	1.07	−10.40–35.00
	Center point of curve	−7.30	1.61	−30.75–15.40	34.60	7.23	−11.40–35.05
	Circle-straight point	−7.00	1.43	−30.75–16.40	34.55	3.56	−11.40–35.10
30	Straight-circle point	−6.90	0.56	−29.20–12.40	28.30	1.10	−10.40–35.00
	Center point of curve	−7.25	1.45	−29.20–14.40	34.60	4.86	−9.40 –35.10
	Circle-straight point	−7.10	1.36	−30.75–15.40	34.55	3.78	−11.40–35.10

Table 3.
Maximum wear, position and range at characteristic points of *R*250 m small radius curve

The following conclusions can be drawn from Figure 11 and Table 3.

(1) When the same number of vehicles passes through *R*250 m small radius curve, the wear severity at the outer rail of the curve decreases in the order of the center point > the circle-straight point > the straight-circle point.

(2) When one million vehicles/trains pass by, the inner rail wear at the straight-circle point is 0.99 mm with the maximum wear speed of 15 km · h^{-1} and the outer rail wear is 1.10 mm with the maximum wear speed of 30 km · h^{-1}; inner and outer rail wear at the center point of the curve is 1.67 mm and 7.40 mm, respectively, with the maximum wear speed of 15 km · h^{-1}; the maximum inner rail wear at the circle-straight point is 1.47 mm with the maximum wear speed of 15 km · h^{-1} and the outer rail wear is 3.78 mm with the maximum wear speed of 30 km · h^{-1}.

(3) As the number of vehicles/trains passing through *R*250 m curve at different speeds goes up, the maximum inner rail wear at straight-circle point locates in −8.35–−6.90 mm range with an average of −7.44 mm and the maximum outer rail wear locates near 28.00 mm; the maximum inner rail wear at center point locates in −7.45–−6.80 mm range with an average of −7.08 mm and the maximum outer rail wear locates in 27.60–34.60 mm range with an average of 34.43 mm; the maximum inner rail wear at circle-straight point locates in −7.40–−6.90 mm range with an average of −7.20 mm and the maximum outer rail wear locates in 27.95–34.55 mm range with an average of 29.56 mm (with the exception of a few working scenarios). Generally speaking, the maximum inner rail wear locates at −7.24 mm on average and the maximum outer rail wear locates at 29.56 mm on average.

(4) When vehicles pass through *R*250 m curve at different speeds, the range of rail wear decreases with the increase of vehicle speed: The inner rail wear at straight-circle point locates in −30.00–28.15 mm range and the outer rail wear locates in −17.40–35.05 mm range; the inner rail wear at center point locates in −30.75–16.40 mm range and the outer rail wear locates in −15.40–35.10 mm range; the inner rail wear at circle-straight point locates in −30.75–16.40 mm range and the outer rail wear locates in −15.40–35.10 mm range.

3.4 R300 m small radius curve in Taiyuan South Station

Figure 12 shows the accumulative rail wear when different numbers of vehicles pass through the straight-circle point, center point and circle-straight point of R300 m small radius curve in EMU depot of Taiyuan South Station at 30 km h^{-1}. It can be seen from Figure 12 that the maximum inner and outer rail wears mainly locate in 26−35 mm range, which has entered the connecting arc between rail top and rail side; there are two wear waveforms on inner and outer rails; rail wear increases as more vehicles/trains pass by.

Figure 13 shows the maximum accumulative rail wear when different numbers of vehicles pass through the straight-circle point, center point and circle-straight point of R300 m small radius curve in EMU depot of Taiyuan South Station at different speeds; Table 4 shows the maximum rail wear, position and range at the straight-circle point, center point and circle-straight point of *R*300 m small radius curve when the number of vehicles/trains passing through the curve reaches the limit.

The following conclusions can be drawn from Figure 13 and Table 4.

(1) When the same number of vehicles passes through *R*300 m small radius curve, the wear severity at the outer rail of the curve decreases in the order of the center point > circle-straight point > the straight-circle point.

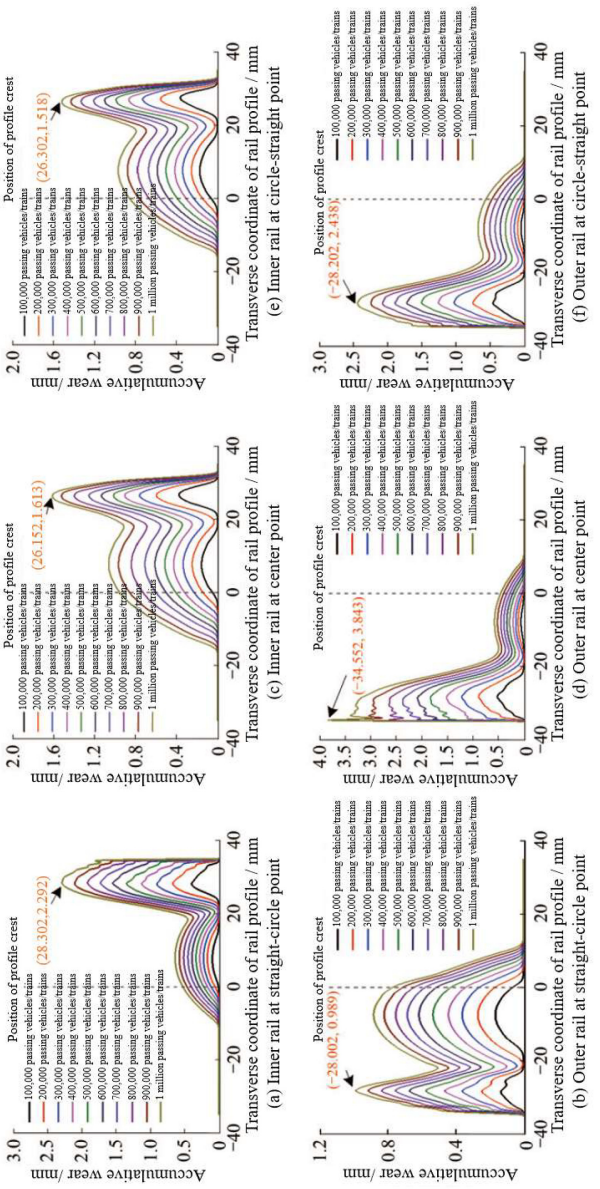

Figure 12.
Accumulative rail wear when different numbers of vehicles pass through *R*300 m small radius curve

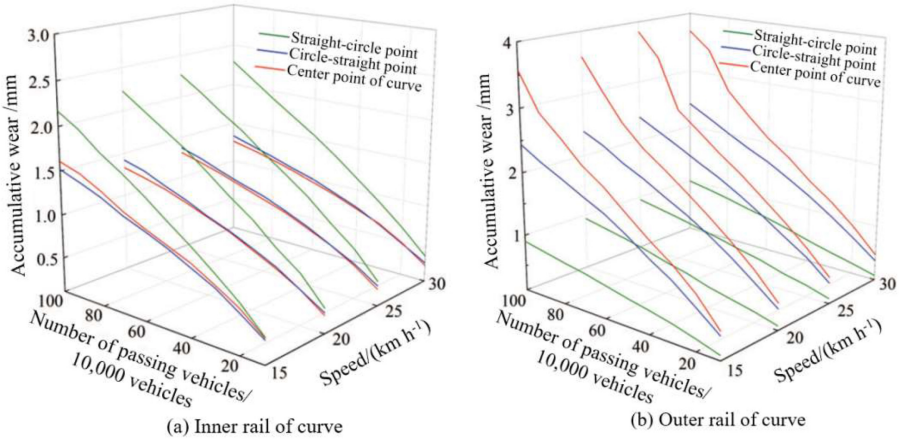

Figure 13.
Accumulative rail wear of *R*300 m small radius curve

		Inner rail of curve			Outer rail of curve		
Speed/(km h−1)	Characteristic point of curve	Position of maximum wear/mm	Maximum wear/mm	Wear range/mm	Position of maximum wear/mm mm	Maximum wear/mm	Wear range/mm
15	Straight-circle point	28.15	2.17	−15.40–35.05	−7.35	0.90	−34.95–15.40
	Center point of curve	26.15	1.61	−20.40–34.15	−34.55	3.57	−35.05 –13.40
	Circle-straight point	26.30	1.52	−7.40–33.75	−28.20	2.44	−35.05–13.40
20	Straight-circle point	28.30	2.23	−11.40–35.05	−28.00	0.94	−34.95–15.40
	Center point of curve	26.00	1.33	−17.40–33.75	−34.60	3.60	−35.10–13.40
	Circle-straight point	26.15	1.42	−15.40–33.75	−28.50	2.40	−35.05–10.40
25	Straight-circle point	28.35	2.27	−14.40–35.05	−28.00	0.95	−34.95–15.40
	Center point of curve	25.90	1.31	−17.40–33.25	−34.55	3.84	−35.05–12.40
	Circle-straight point	26.20	1.37	−15.40–33.75	−28.40	2.40	−35.05–9.35
30	Straight-circle point	28.30	2.29	−13.35–35.05	−28.00	0.99	−34.95–14.40
	Center point of curve	25.90	1.26	−16.40–33.25	−34.55	3.70	−35.05–11.35
	Circle-straight point	26.15	1.33	−14.40–33.75	−28.80	2.41	−35.05–8.40

Table 4.
Maximum wear, position and range at characteristic points of *R*300 m small radius curve

(2) When one million vehicles/trains pass by, the inner and outer rail wear at the straight-circle point is 2.29 and 0.99 mm, respectively, with the maximum wear speed of 30 km · h^{-1}; inner rail wear at the center point of the curve is 1.61 mm with the maximum wear speed of 15 km · h^{-1} and the outer rail wear is 3.84 m with the maximum wear speed of 25 km · h^{-1}; the inner and outer rail wear at the circle-straight point is 1.52 and 2.44 mm, respectively, with the maximum wear speed of 15 km · h^{-1}.

(3) As the number of vehicles/trains passing through *R*300 m curve at different speeds goes up, the maximum inner rail wear at straight-circle point locates in 27.95–28.35 mm range and the maximum outer rail wear locates in −28.10–−7.25 mm range; the maximum inner rail wear at center point locates in 25.90–26.80 mm range and the maximum outer rail wear locates in −34.60–−28.05 mm range; the maximum inner rail wear at circle-straight point locates in 26.15–27.50 mm range and the maximum outer rail wear locates in −28.80–−27.95 mm range. Generally speaking, the maximum inner rail wear locates at 27.07 mm on average and the maximum outer rail wear locates at −25.07 mm on average.

(4) When vehicles pass through *R*300 m curve at different speeds, the range of rail wear decreases with the increase of vehicle speed: The inner rail wear at straight-circle point locates in −11.40~35.05 mm range and the outer rail wear locates in −34.9523–15.3977 mm range; the inner rail wear at center point locates in −20.3977–34.1523 mm range and the outer rail wear locates in −35.1023–13.3977 mm range; the inner rail wear at circle-straight point locates in −17.3977–33.7523 mm range and the outer rail wear locates in −35.0523–13.3977 mm range.

3.5 Influence of rail wear on dynamics characteristics

Rail wear increases as more trains run by, altering the wheel-rail contact relation. In other words, wheel-rail contact changes from initial elliptical contact to multipoint non-elliptical contact, thus changing the dynamics performance of the vehicle. For the analysis the change of dynamics performance with the increase of rail wear, the paper looks into the influence of rail wear on dynamics characteristics of the vehicle in three working conditions of the rail (namely, original profile, profile as 500,000 vehicles/trains pass by and that as one million vehicles/trains pass by) on the premise that the operation speed is set at 30 $km \cdot h^{-1}$.

Under the presumption that the profiles at both ends of line *L* are *i* and *j*, respectively, the profile at any point *x* within the range of Line *L* is generated by linear transition of *i* and *j*, as shown in Figure 14.

Figures 15–18 show the change of derailment coefficient, reduction rate of wheel load, vertical and lateral wheel-rail force at No. 1 wheelset position of the train-track system in EMU depots of Guangzhou East Station and Taiyuan South Station.

It can be seen from Figures 15–18 that the influence of rail wear on lateral wheel-rail force and derailment coefficient is minor when the train enters the first curve and its straight section, but such influence is amplified with greater difference noticed when the train passes through the first curve; rail wear has no significant effect on vertical wheel-rail force and reduction rate of wheel load; when the number of passing vehicles reaches 1 million, the derailment coefficient of the outer rail of the line in EMU depot of Guangzhou East Station will

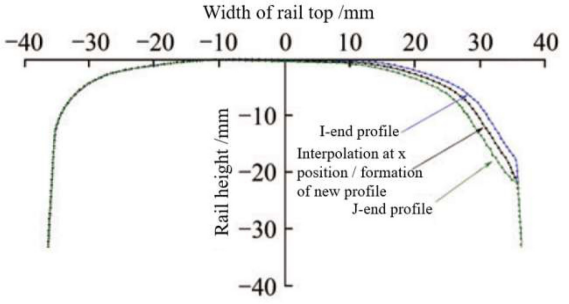

Figure 14.
Profile generation at certain position within the range of Line L

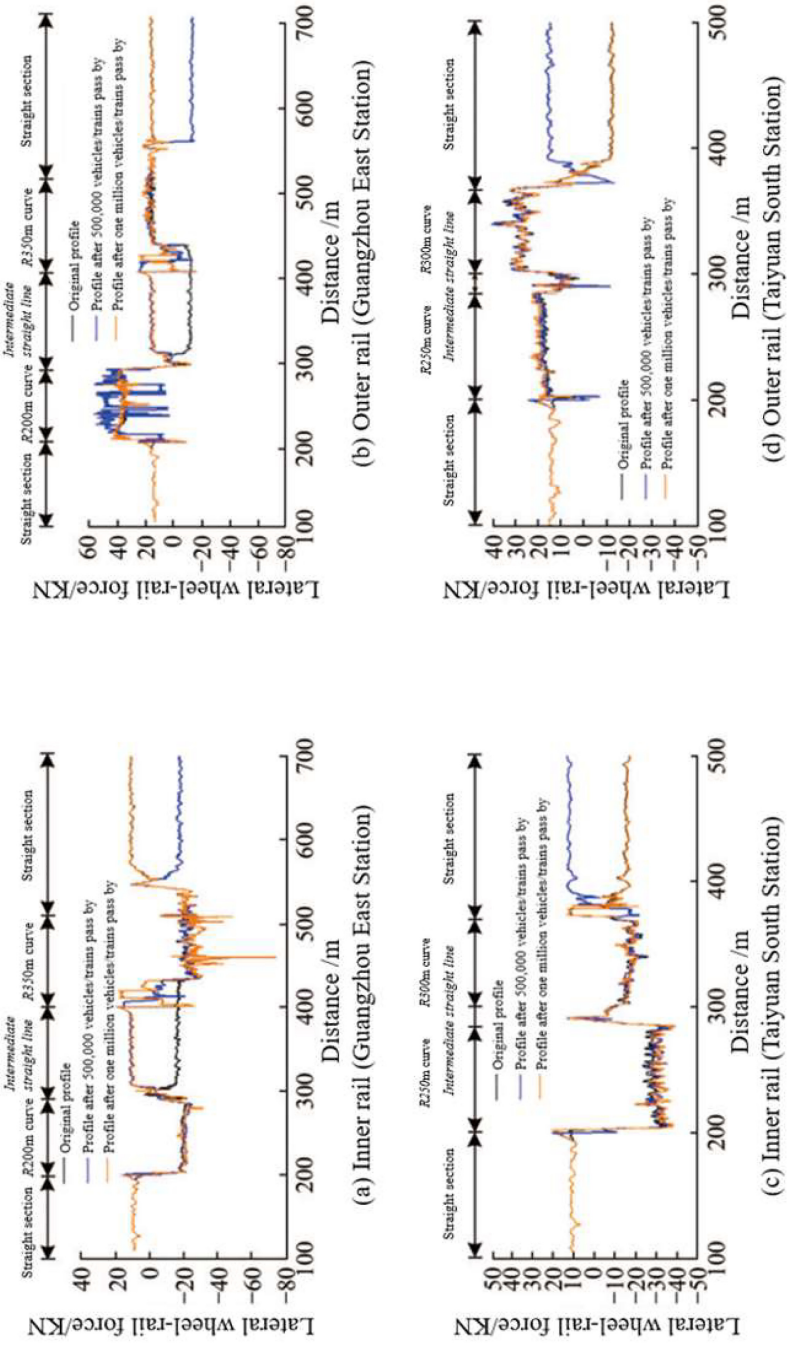

Figure 15.
Variation curve of lateral wheel-rail force along line

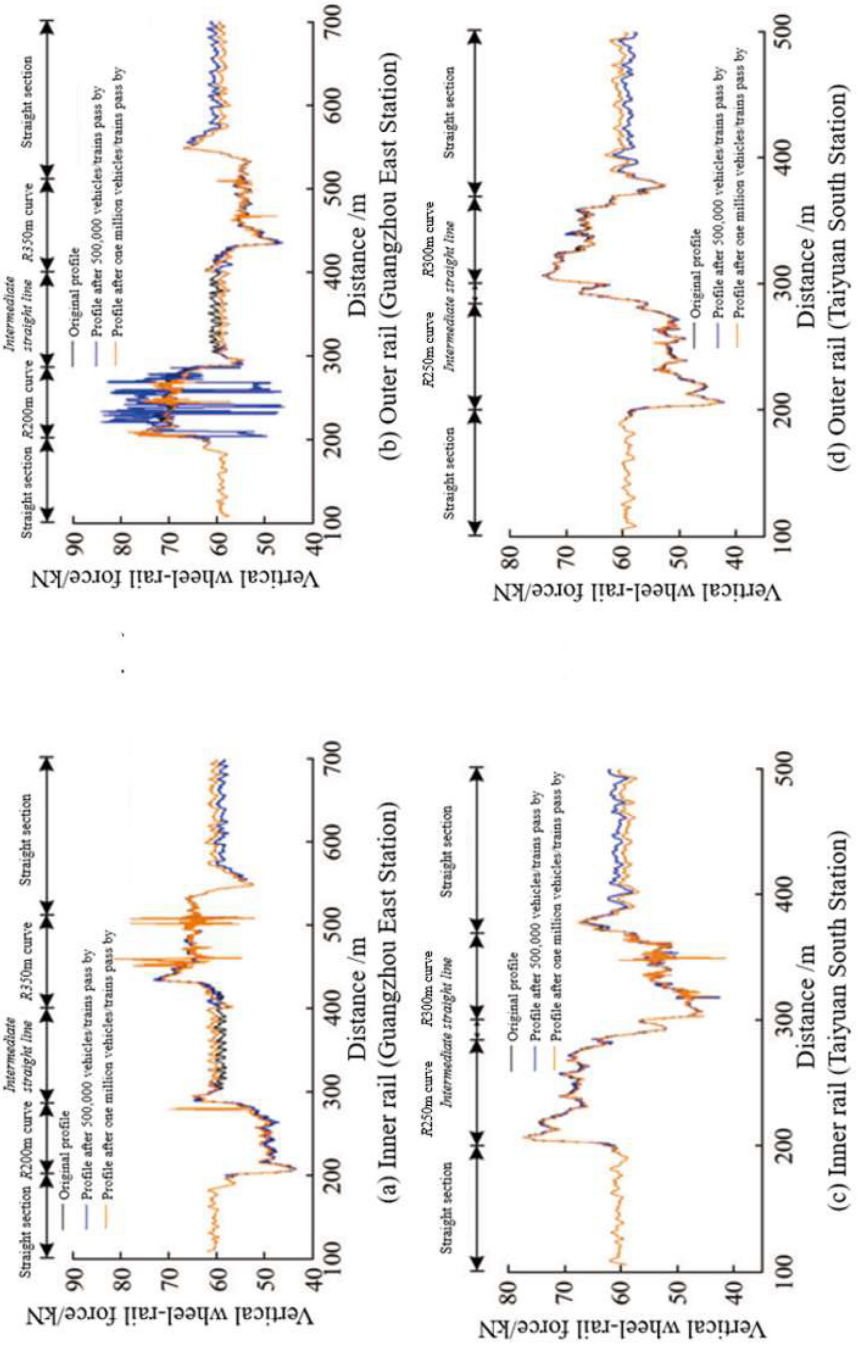

Figure 16.
Variation curve of vertical wheel-rail force along line

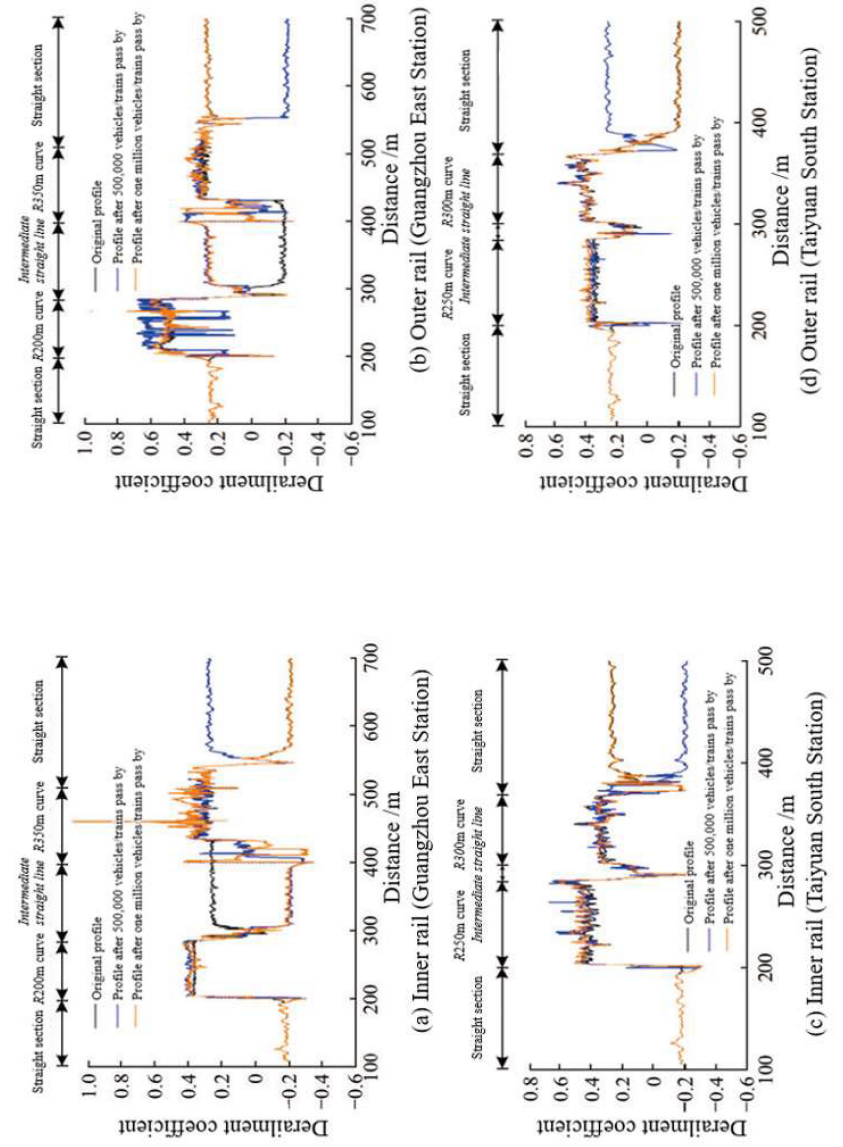

Figure 17.
Variation curve of derailment coefficient along line

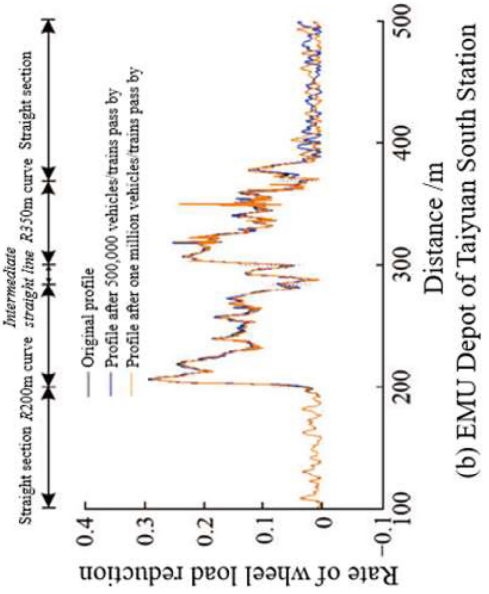

(b) EMU Depot of Taiyuan South Station

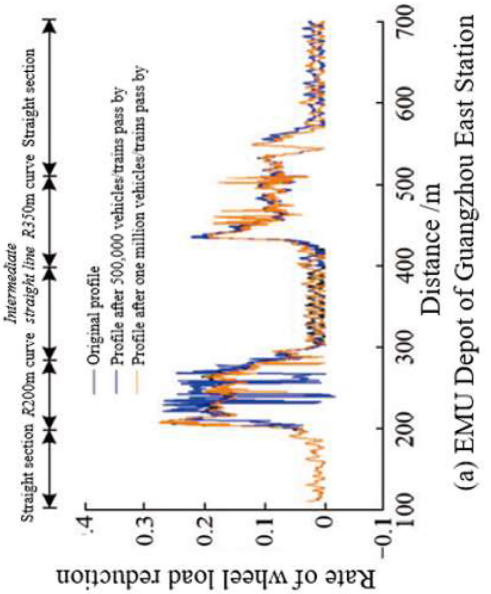

(a) EMU Depot of Guangzhou East Station

Figure 18.
Variation curve of reduction rate of wheel load along line

exceed 0.8, the limit specified in the specification for dynamic inspection. In this case, the train shall pass through the line at decelerated speed to prevent derailment; the derailment coefficient is set at 0.7 on the line of EMU depot of Taiyuan South Station.

4. Conclusion

(1) The wear severity at the straight-circle point, center point and circle-straight point of small radius curve with no transition curve follows the order of the center point > the circle-straight point > the straight-circle point. Accumulative wear deteriorates as more trains run by.

(2) In the case of small radius curve, uneven wear tends to be noticed at both sides of the rail, while two wear formworks, a big one and a small one, are generally obtained at both sides of the connecting points of arcs with different radii on the top of the rail on side one or sides two, in which the small radius arc of the rail corresponds to the large waveform, while the large radius arc, the small waveform.

(3) When the number of passing vehicles/trains reaches 1 million, the maximum inner rail wears of *R*200 m, *R*250 m, *R*300 m and *R*350 m curves locates at 7.00, −7.05, 28.30 and −6.80 mm, respectively, with the corresponding maximum wears of 1.88, 1.67, 2.29 and 1.32 mm, respectively. The maximum outer rail wears are found at −34.65, 34.60, −34.55 and 34.65 mm, respectively, with maximum wears of 10.11, 7.40, 3.84 and 3.12 mm, respectively.

(4) The severity of the accumulative wear at the straight-circle point, center point and circle-straight point of the curve with different radii declines in the order of *R*200 m, *R*250 m, *R*300 m and *R*350 m curves.

(5) When vehicles/trains pass through small radius curves at different speeds, the range of rail wear decreases with the increase of speed; when the number of passing vehicles reaches 1 million, the inner rail wears of *R*200 m, *R*250 m, *R*300 m and *R*350 m curves are found in −23.40–32.15, −30.75–28.15, −20.40–34.15 and −33.25–32.00 mm ranges, respectively, and the outer rail wears locate in −35.05–17.40, −17.40–35.10, −35.10–15.40 and −18.40–35.10 mm ranges, respectively, with the straight-circle point recording the largest range of wear, followed by the center point and the circle-straight point.

(6) The dynamics performance of the vehicle/train increases with the development of rail wear, but it exerts only limited impact overall. The wear of the curve line mainly affects lateral wheel-rail force and derailment coefficient. When the number of passing vehicles reaches 1 million, the derailment coefficient caused by rail wear in EMU depot of Guangzhou East Station exceeds 0.8, the limit specified in the specification. The coefficient stands at 0.7 on the line of Taiyuan South Railway Station. Therefore, when the rail is worn to a certain extent, the vehicle shall pass through the line in EMU depot of Guangzhou East Station at decelerated speed to prevent derailment.

References

Asih, A., Ding, K., & Kapoor, A. (2012). Modelling rail wear transition and mechanism due to frictional heating. *Wear*, *284/285*, 82–90.

Dang, V., & Maitournam, M. (2002). On some recent trends in modelling of contact fatigue and wear in rail. *Wear*, *253*(1/2), 219–227.

Deters, L., & Proksch, M. (2004). Friction and wear testing of rail and wheel material. *Wear*, *258*(7), 981–991.

Ding, J., Lewis, R., Beagles, A., & Wang, J. (2018). Application of grinding to reduce rail side wear in straight track. *Wear*, *402/403*, 71–79.

Feng, Z. (2018). *Study on the Operation Safety and the Rail Wear About EMU Passing through Small Radius Curves*. Beijing: China Academy of Railway Sciences.

Hu, Y., Zhou, L., Ding, H. H., Tan, G. X., Lewis, R., Liu, Q. Y., Guo, J., & Wang, W. J. (2020). Investigation on wear and rolling contact fatigue of wheel-rail materials under various wheel/rail hardness ratio and creepage conditions. *Tribology International*, *143*, 1–14.

Jendel, T., & Berg, M. (2002). Prediction of wheel profile wear. *Vehicle System Dynamics*, *37*(Supplement 1), 502–513.

Kalker, J. (1990). *Three-dimensional Elastic Bodies in Rolling Contact*. Dordrecht: Kluwer Academic Publishers.

Khan, S. A., Persson, I., Lundberg, J., & Stenstrom, C. (2017). Prediction of top-of-rail friction control effects on rail RCF suppressed by wear. *Wear*, *380/381*, 106–114.

Lewis, R., & Olofsson, U. (2009). *Wheel-rail Interface Handbook*. Florida: CRC Press.

Lewis, R., Christoforou, P., Wang, W. J., Beagles, A., Burstow, M., & Lewis, S. R. (2019). Investigation of the influence of rail hardness on the wear of rail and wheel materials under dry conditions (ICRI wear mapping project). *Wear*, *430/431*, 383–392.

Lin, F. (2014). *Research on Wheel Wear and wheel Profile Optimization of High Speed Train*. Beijing: China Academy of Railway Sciences.

Meehan, P., Daniel, W., & Campey, T. (2005). Prediction of the growth of wear-type rail corrugation. *Wear*, *258*(7/8), 1001–1013.

Olofsson, U., & Telliskivi, T. (2003). Wear, plastic deformation and friction of two rail steels—a full-scale test and a laboratory study. *Wear*, *254*(1), 80–93.

Pavlík, A., Gerlici, J., & Lack, T. (2019). Prediction of the rail-wheel contact wear of an innovative bogie by simulation analysis. *Transportation Research Procedia*, *40*, 855–860.

Piotrowski, J., & Chollet, H. (2005). Wheel-rail contact models for vehicle system dynamics including multi-point contact. *Vehicle System Dynamics*, *43*(6/7), 455–483.

Ramalho, A. (2015). Wear modelling in rail-wheel contact. *Wear*, *330/331*, 524–532.

Sladkowski, A., & Sitarz, M. (2004). Analysis of wheel-rail interaction using fesoftware. *Wear*, *258*(7/8), 1217–1223.

Su, C., Shi, L. B., Wang, W. J., Wang, D. Z., Cai, Z. B., Liu, Q. Y., & Zhou, Z. R. (2019). Investigation on the rolling wear and damage properties of laser dispersed quenched rail materials treated with different ratios. *Tribology International*, *135*, 488–499.

Wang, P., Wang, C., Wang, W., & Liu, Q. (2011). Application of GA-BP ANN in the prediction of wear volumes of rail steel. *Lubrication Engineering*, *36*(2), 99–102.

Zhao, G., & Zeng, S. (1995). Effect of curve radius and off-balance superelevation on side wear of high rail on curved track. *China Railway Science*, *16*(3), 90–96.

Zhu, B., Zeng, J., Zhang, D., & Yi, W. (2019). A non-hertzian wheel-rail contact model considering wheelset yaw and its application in wheel wear prediction. *Wear*, *432/433*, 1–8.

Zou, D., Yang, Q., Lu, G., & Xing, L. (2010). *Failure Analysis and Damage Map of Rail*. Beijing: China Railway Publishing House in Chinese.

Corresponding author
Hao Li can be contacted at: 357469456@qq.com